Applied Catalysis B: Environmental 92 (2009) 90–99

Contents lists available at ScienceDirect

Applied Catalysis B: Environmental

journal homepage: www.elsevier.com/locate/apcatb

# Ru-based catalysts for glycerol hydrogenolysis—Effect of support and metal precursor

E.S. Vasiliadou [a], E. Heracleous [b], I.A. Vasalos [b], A.A. Lemonidou [a,b,*]

[a] Department of Chemical Engineering, Aristotle University of Thessaloniki, P.O. Box 1517, University Campus, GR-54124 Thessaloniki, Greece
[b] Chemical Process Engineering Research Institute (CERTH/CPERI), P.O. Box 60361 Thermi, Thessaloniki 57001, Greece

ARTICLE INFO

*Article history:*
Received 12 May 2009
Received in revised form 14 July 2009
Accepted 20 July 2009
Available online 25 July 2009

*Keywords:*
Glycerol
Hydrogenolysis
Ruthenium
Acidity
1,2-propanediol

ABSTRACT

Hydrogenolysis of biomass-derived glycerol is an alternative route for the production of value-added chemicals, such as 1,2-propanediol. Ru-based ($\gamma$-$Al_2O_3$, $SiO_2$, $ZrO_2$) catalysts were prepared by the wet impregnation method and evaluated in glycerol hydrogenolysis at 240 °C and 8 MPa $H_2$. The effect of the refractory oxide and metal precursor ($RuCl_3{\cdot}xH_2O$, $RuNO(NO_3)_3$) used for catalyst preparation was examined. The nature of the oxidic support was found to influence the ability of the catalyst to both activate the glycerol substrate and selectively convert it to propanediol. Among the tested catalysts, Ru/$Al_2O_3$ prepared with the chloride precursor exhibited the highest activity (69%) and the lowest selectivity to 1,2-propanediol due to excessive hydrogenolysis of 1,2-propanediol to 1-propanol. Ru/$SiO_2$ prepared with the nitrate precursor yielded to the highest selectivity to 1,2-propanediol (65%) at 20% conversion level. The characterization of the catalytic materials revealed a correlation between catalytic activity for the hydrogenolysis reaction and total acidity, as the yield to hydrogenolysis products increased with the concentration of the acid sites. The use of different metal precursors affected the catalytic activity and product selectivity mainly in the case of $\gamma$-$Al_2O_3$ used as support, but with $SiO_2$ support as well. The supported Ru samples prepared using the chloride precursor showed higher activity compared to the corresponding materials prepared with nitrate, but selectivity to 1,2-propanediol was lower due to the promotion of excessive hydrogenolysis to propanols. These effects were attributed to the retention of $Cl^-$ ions on the support surface, as evidenced by TEM-EDS.



## 1. Introduction

Biodiesel derived from vegetable oils and animal fats has received considerable attention in recent years. In the transport sector, it may be effectively used in diesel engines, both blended with fossil diesel fuel and in pure form [1]. Biodiesel has been produced on an industrial scale in the European Union since 1992 due to environmental concerns and EU agro fuels incentives. Worldwide biofuels demand is predicted to increase up to 98 million tonnes in 2011 with an annual increase (growth) rate 20% [2].

Biodiesel consists of fatty acid methyl esters produced via the transesterification of triglycerides with methanol in the presence of basic or acidic catalysts. For every 9 kg of biodiesel produced, about 1 kg of crude glycerol by-product is also formed [3]. This crude glycerol could serve as a renewable feedstock for the chemical industry, replacing fossil-derived products. Finding new uses for glycerol would make biodiesel production a cost effective process. In addition, glycerol has been identified by the U.S. Department of Energy as one of the top-12 building block chemicals that can be derived from sugars and converted to high-value bio-based chemicals or materials [4].

The hydrogenolysis of glycerol to 1,2- and 1,3-propanediol is an attractive innovative pathway for the production of renewable value-added chemicals. 1,2-propanediol (1,2-PDO) is a major commodity chemical with a 4% annual market growth. Typical uses of 1,2-propanediol are in unsaturated polyester resins, functional fluids, pharmaceuticals/cosmetics, paints, etc. 1,3-Propanediol is mainly used for the production of polyesters via co-polymerization with terephthalic acid. These two products are currently produced from petroleum derivatives such as propylene oxide (1,2-propanediol) and ethylene oxide or acrolein (1,3-propanediol) by chemical catalytic routes [4–6]. Their production from renewable glycerol could potentially offer great environmental benefits.

Glycerol hydrogenolysis takes place under high hydrogen pressures and mild temperatures in the presence of suitable catalytic materials. Initial $H_2$ pressures of 0.5–10 MPa and temperatures of 120–240 °C have been reported in literature [7–20] and patents [21–23]. The hydrogenolysis reaction is suggested to proceed via dehydration of glycerol to acetol and 3-hydroxypropanal by acid catalysis and subsequent hydrogenation to the

* Corresponding author at: Department of Chemical Engineering, Aristotle University of Thessaloniki, P.O. Box 1517, University Campus, GR-54124 Thessaloniki, Greece. Tel.: +30 2310 996273; fax: +30 2310 996184.
*E-mail address:* alemonidou@cheng.auth.gr (A.A. Lemonidou).

0926-3373/$ – see front matter © 2009 Elsevier B.V. All rights reserved.
doi:10.1016/j.apcatb.2009.07.018

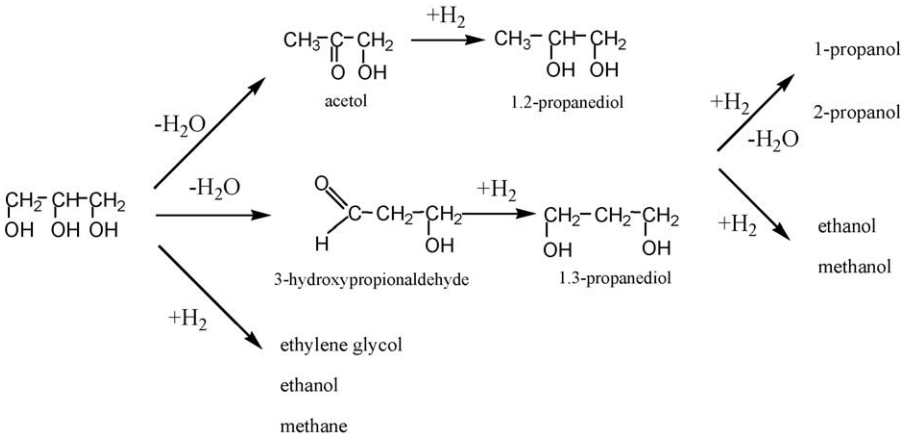


**Scheme 1.**

glycols by metal catalysts [14,17–19], as shown in Scheme 1. Another mechanism proposed by Montassier et al. [24] for this reaction involves dehydrogenation of glycerol to glyceraldehyde followed by dehydration to 2-hydroxyacrolein and hydrogenation to 1,2-propanediol with a Ru/C catalyst under neutral/slightly basic aqueous polyol solutions. Besides the hydrogenolysis reaction, degradation reactions involving C–C breaking also occur. The products from C–C cracking are mainly ethylene glycol, methanol, ethanol and methane. Therefore, the selective conversion of glycerol to propanediols requires a suitable catalyst with bifunctional acid sites/metal surface, favouring the cleavage of the glycerol C–O bonds (dehydration/hydrogenation) by hydrogen and eliminating C–C bond scission.

Many supported metal catalysts have been reported for this type of reaction in liquid phase. Tomishige and co-workers reported the use of supported group VIII metal (especially Ru/C and Rh/$SiO_2$) catalysts in combination with a strong solid acid (Amberlyst 15,70) at mild temperatures of 120 °C and $H_2$ pressures of 4–8 MPa [14,17–19]. Other studies have demonstrated the use of Ru-supported catalysts on supports like carbon [15], $TiO_2$ [12,20] and acidic heteropoly salts [9]. Feng et al. [12] investigated the effect of various supports ($TiO_2$, $SiO_2$, NaY, γ-$Al_2O_3$ and active-carbon) on Ru catalysts and found that the support material can influence the metal particle size and the reaction routes, with $TiO_2$ yielding the most active and $SiO_2$ the most selective catalyst for propanediol production. Catalysts like Rh/C [6] and Pt/$WO_3$/$ZrO_2$ [10] have also been used in an attempt to selectively produce 1,2- and especially 1,3-propanediol. In addition, metals like copper-chromite [7] have been evaluated for low pressure hydrogenolysis of glycerol and Cu–ZnO [8] for selective production of 1,2-propanediol.

In this work, the hydrogenolysis of glycerol was investigated on supported Ru catalysts, with a metal loading of 5 wt% Ru. The scope was to study the effect of the support material (γ-$Al_2O_3$, $SiO_2$, $ZrO_2$) on the structure and physicochemical characteristics of the catalysts, as well as the performance in the glycerol hydrogenolysis reaction. In addition, the use of two different ruthenium precursors for the preparation of the catalysts, chloride and nitrate, and their effect on the properties and catalytic performance of the Ru-supported catalysts was investigated.

## 2. Experimental

### 2.1. Catalyst preparation

Supported 5 wt% Ru catalysts were prepared using the wet impregnation method. $SiO_2$ (Saint-Gobain, Norpro, $S_{BET}$ = 106 $m^2\ g^{-1}$), $ZrO_2$ (Norton, $S_{BET}$ = 88.7 $m^2\ g^{-1}$) and γ-$Al_2O_3$ (Saint-Gobain, Norpro $S_{BET}$ = 211 $m^2\ g^{-1}$) were used as the support material. The supports were crushed and sieved to a powder form of 45 $< d_p <$ 106 μm. Ruthenium was loaded on the supports using two different precursors: $RuCl_3 \cdot xH_2O$ (Next Chimic) and $RuNO(NO_3)_3$ (Alfa-Aesar). After impregnation the slurry was stirred at 70 °C for 1 h in a rotary evaporator and then the solvent was removed at 80 °C under mild vacuum. The catalysts were then dried for 17 h at 120 °C and calcined in synthetic air for 3 h at 500 °C.

The catalysts are referred to as RuS(X), where S indicates the support (Al, Si, Zr) and X the Ru precursor used for the preparation ($Cl_3$, $NO_3$).

### 2.2. Catalyst characterization

Surface areas of the samples were determined by $N_2$ adsorption at 77 K, using the multipoint BET analysis method, with an Autosorb-1 Quantachrome flow apparatus. Prior to the measurements, the samples were dehydrated in vacuum at 250 °C overnight.

X-ray diffraction (XRD) patterns were obtained using a Siemens D500 diffractometer, with Cu Kα radiation. The Scherrer equation was used to calculate the crystal size of the metal particles from the X-ray patterns.

The morphology of the synthesized materials was examined by scanning electron microscopy (SEM) on a JEOL 6300 microscope, coupled with energy-dispersive X-ray analysis (EDX; Oxford Link ISIS-2000) for local elemental composition determination.

Structural characterization and dispersion measurements of the catalytic materials using high resolution transmission electron microscopy (HRTEM) coupled with energy-dispersive X-ray analysis (EDS) was performed. The samples were reduced in 10%$H_2$/He flow at 350 °C before analyzing. Electron microscopy experiments were carried out in a JEOL 2011 high resolution transmission electron microscope, operating at 200 kV, with a point resolution of 0.23 nm and $C_s$ = 1.0 mm. The microscope is also fitted with an Oxford Instruments INCAx-sight liquid nitrogen cooled EDS detector with an Si(Li) window for detailed elemental analysis of the catalysts. Processing of the spectra was accomplished using the INCA Microanalysis Suite version 4.02 software. HRTEM was used to calculate particle size and dispersion using the equation $D = 1.32/d_{ave}$, where $D$ = dispersion and $d$ = average metal particle size (nm) [25].

The dispersion of the catalysts was also measured with hydrogen chemisorption and subsequent temperature programmed desorption of the chemisorbed hydrogen. These experiments were performed in a gas flow system equipped with a

quadrupole mass analyzer (Omnistar, Balzers). Typically, the catalyst sample (100 mg) was placed in a U-shaped quartz reactor and pretreated in flowing He (30 $cm^3$/min) for 0.5 h at 250 °C, followed by cooling at room temperature. Temperature was increased to 350 °C in a 10% $H_2$/He flow (30 $cm^3$/min) to complete the reduction and then hydrogen chemisorption was performed at 250 °C under hydrogen flow (25 $cm^3$/min, 100% $H_2$) for 1 h. The sample was then cooled to room temperature under constant hydrogen flow. At room temperature the catalyst was purged in a He flow of 60 $cm^3$/min for 2.5 h. The TPD experiments were performed by heating the sample at a rate of 10 °C/min from room temperature to 700 °C, under a He flow of 30 $cm^3$/min. Dispersion values were calculated from quantification of the desorbed hydrogen and the assumption that the stoichiometry factor between chemisorbed hydrogen and surface Ru equals H:Ru = 1:1.

The reduction characteristics of the catalysts were studied by temperature programmed reduction (TPR) using the same apparatus and pretreatment method as for the $H_2$-TPD measurements. After pretreatment, the temperature was raised from room temperature to 350 °C at a rate of 10 °C/min in a 10% $H_2$/He flow (30 $cm^3$/min). The main ($m/z$) fragments registered were $H_2$ = 2, $H_2O$ = 18, 17, 16, He = 4, $O_2$ = 32 and $N_2$ = 28.

$NH_3$ temperature programmed desorption (TPD) was used to determine the acid properties of the catalytic materials. The experiments were conducted on the same apparatus as the TPD experiments described above. The catalysts (100 mg) were pretreated at 250 °C for 0.5 h and then cooled to 100 °C under a 30 $cm^3$/min He flow. The pretreated samples were saturated with 5% $NH_3$/He for 1 h at 100 °C, with subsequent flushing with helium at 100 °C for 2 h to remove the physisorbed ammonia. TPD analysis was carried out from 100 to 700 °C at a heating rate of 10 °C/min. The following ($m/z$) fragments were registered: $NH_3$ = 15, $H_2O$ = 18, $N_2$ = 28, NO = 30, $N_2O$ = 44, and $NO_2$ = 46. Quantitative analysis of the desorbed ammonia was based on ($m/z$) 15.

### 2.3. Activity test

Glycerol hydrogenolysis was carried out in a 450 ml stainless-steel batch reactor (Parr Instruments) equipped with an electronic temperature controller, a mechanical stirrer and a tube for the sampling of the liquid phase. Reaction was normally conducted under the following standard conditions: 240 °C temperature, 8 MPa initial hydrogen pressure, 0.9 g catalyst weight, 120 ml pure glycerol feedstock volume, 5 h reaction time and 1000 rpm stirring speed.

The reaction sequence was as follows: loading of the reactor with pure glycerol and the appropriate amount of catalyst, $N_2$ flushing for 10 min at 0.2 MPa, $H_2$ flushing for 5 min at 0.5 MPa and increase of temperature and $H_2$ pressure to the desired conditions under constant stirring. The reaction was allowed to run for 5 h under the above mentioned conditions during which liquid samples were periodically removed. After each sampling the reactor was back filled with hydrogen to retain the pressure constant. After 5 h the system was allowed to cool down to room temperature and the gas products were collected in a gas bag.

Liquid samples were analyzed by GC (Varian 3300, FID, DB-Wax 30 m × 0.53 mm × 1.0 μm) and identified by GC-MS (DB-Wax 30 m × 0.53 mm × 1.0 μm). N-butanol was used as a solvent for the GC analysis. The multiple point internal standard method was used for the quantification of conversion and selectivity determination. Gas analysis was performed in Varian 3700 (TCD, Porapak Q, MS-5A). The liquid products detected were: 1,2-propanediol, 1,3-propanediol, ethylene glycol, hydroxyacetone (acetol), 1-propanol, 2-propanol, ethanol, methanol. The conversion and selectivity was calculated using the following equations:

$$\text{conversion} = \frac{\text{moles glycerol (out)} - \text{moles glycerol (in)}}{\text{moles glycerol (in)}} \times 100$$

$$\text{liquid-based selectivity} = \frac{\text{moles of C in liquid product } i}{\text{moles of C in all liquid products}} \times 100$$

The carbon balance in all experiments was better than 100 ± 5%.

## 3. Results and discussion

### 3.1. Catalyst characterization

The main physicochemical characteristics of the Ru-supported catalysts are summarized in Table 1. Independent of the refractory oxide, the deposition of Ru causes a slight decrease in the specific surface area of the samples compared to the corresponding supports. Moreover, comparison of the surface area of the samples before and after reaction reveals a decrease in the surface area of the used catalysts, mainly in the case of the $ZrO_2$ supported sample. This decrease can be probably attributed to partial agglomeration of the Ru particles on the catalyst surface, caused by the high pressure conditions and the liquid phase nature of the reaction.

The crystalline phases formed in the fresh catalysts were investigated by X-ray diffraction. Fig. 1 illustrates the diffractograms obtained for all samples with different supports and different precursors. XRD analysis clearly shows the formation of crystalline ruthenium oxide ($RuO_2$) on the as-synthesized materials. The $RuO_2$ lines are difficult to distinguish in the case of the $ZrO_2$ support, as they largely coincide with those of the pure $ZrO_2$ in the baddeleyite crystallographic structure. The diffraction patterns of the nitrate-prepared Ru/(Al, Si) catalysts (Fig. 1: D and G lines) show that the diffraction lines corresponding to the $RuO_2$ phase are slightly more intense on Ru/γ-$Al_2O_3$ than on Ru/$SiO_2$. This indicates an effect of the different support oxide on the size of $RuO_2$ particles, with γ-$Al_2O_3$ favouring a better crystallization and formation of larger $RuO_2$ crystals [26]. The calculated $RuO_2$ particle sizes (Scherrer equation), presented in Table 1, indeed show that on γ-$Al_2O_3$ $RuO_2$ crystals are slighter larger than on $SiO_2$. The size of $RuO_2$ on $ZrO_2$ was impossible to determine, due to the reasons already mentioned. XRD analysis of the used samples (only the XRD pattern of used $RuSiCl_3$ is shown here for brevity) indicates that during reaction the ruthenium active phase is reduced from $RuO_2$ to metallic Ru as expected, since the reaction proceeds under reducing conditions.

**Table 1**
Physicochemical catalyst characterization.

| Catalyst | BET surface area ($m^2 g^{-1}$) | | $RuO_2$ size from XRD (nm) | Ru size (nm) determined by | | Dispersion (%) determined by | | Total acidity. (μmol $NH_3 g^{-1}$) |
|---|---|---|---|---|---|---|---|---|
| | Fresh | Used | | TEM | $H_2$-TPD | TEM | $H_2$-TPD | |
| RuAl($Cl_3$) | 195.8 | 176 | 15.17 | 14.46 | 8.2 | 9.12 | 16.1 | 28 |
| RuAl($NO_3$) | 190.6 | 177 | 17.61 | 13.55 | 1.9 | 9.74 | 68.4 | 19 |
| RuSi($Cl_3$) | 97.0 | 95.3 | 9.27 | 8.23 | n.d. | 16.04 | n.d. | 18 |
| RuSi($NO_3$) | 98.3 | 89.9 | 13.57 | 8.17 | n.d. | 16.16 | n.d. | 13 |
| RuZr($NO_3$) | 75.7 | 53.7 | n.d. | 5.5 | 1.5 | 24.0 | 86.8 | 21 |

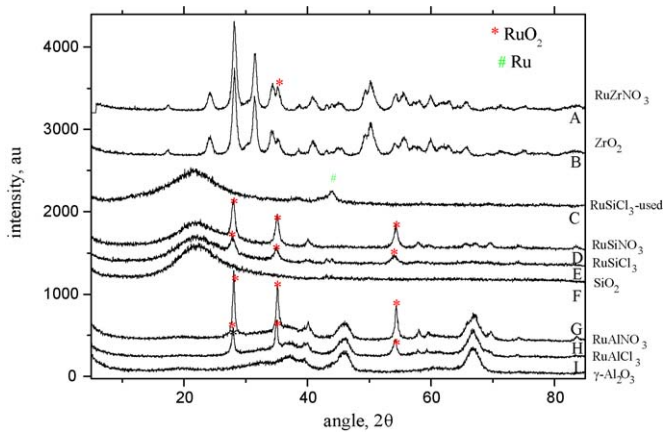


**Fig. 1.** XRD patterns of supported Ru catalysts.

SEM-EDS was used in order to observe the morphology of the catalytic surface as prepared and after testing. Comparing the morphology – coupled with elemental mapping (the micrographs of which are not shown for brevity) of the catalyst surface on the three different supports, we can see that $RuO_2$ particles are smaller and better dispersed on $SiO_2$, than on $\gamma$-$Al_2O_3$ and $ZrO_2$, in accordance with the XRD results which showed the formation of smaller crystals on silica. The catalysts after testing (used samples) do not display any significant changes in surface morphology, at least within the detection capabilities of SEM-EDS. The same applies for the Ru samples prepared with the different metal precursors, chloride and nitrate (the micrographs are not shown).

A more in-depth structural characterization of the Ru catalysts was attempted with high resolution transmission electron microscopy. As described in the experimental section, the as-synthesized supported Ru catalysts were pre-reduced in $H_2$ at 350 °C prior to the analysis, in order to simulate the metallic Ru active species and the state of the catalyst under actual reaction conditions. The EDS analysis of the samples indeed showed the presence of only metallic Ru particles, confirming the total reduction of the $RuO_2$ phase to the metallic Ru state. The TEM images were also used to calculate the size distribution of the Ru particles on the catalysts, the average Ru particle size using a Gaussian analysis fitting and the dispersion of the materials [25] (results tabulated in Table 1).

Representative TEM images of the fresh catalysts prepared with the nitrate Ru precursor and supported on $\gamma$-$Al_2O_3$ and $SiO_2$ and $ZrO_2$ are shown in Fig. 2. Comparison of the three supports reinforces the conclusions drawn by XRD and SEM, as it is apparent that the Ru crystals are smaller, uniform in size and homogeneously distributed on the $SiO_2$ and $ZrO_2$ surface. The shape of ruthenium particles on the surface of all supports was approximately spherical, and the boundary of the ruthenium particles could be clearly observed. The Ru/Si($NO_3$) catalyst exhibits a narrow particle size distribution (Fig. 2), with the mean particle size estimated at 8.17 nm and the dispersion equal to 16.16%. In contrast, on $Al_2O_3$ a wide range of crystal sizes is observed. The size of the Ru particles is clearly in a broader range with a maximum peak at 13.55 nm and some particles bigger than 45–50 nm, while dispersion is calculated to be only equal to 9.74%. Ru/Zr($NO_3$) clearly differs from the two above mentioned samples as $ZrO_2$ support has crystalline structure, with superfine crystals rendering it difficult to distinguish Ru particles. The existence of Ru element was however confirmed with the help of EDX and measurement of d-spacing of the lattice planes (for Ru = 2.05 Å and for $ZrO_2$ = 2.99 Å). Based on these data we were able to detect the presence of Ru particles uniform in size of average value ~5.5 nm and dispersion equal to 24%.

Unlike SEM, TEM analysis reveals a tentative change in the morphology of the catalysts after reaction. Fig. 3 presents TEM micrographs of the fresh and used RuSi($NO_3$) catalyst. This sample was tested in glycerol hydrogenolysis for 5 h and collected after the experiment without further treatment. As shown in Fig. 3, larger metallic Ru particles are observed on the surface after reaction. Careful inspection of the image suggests that the observed Ru particles are agglomerated but not sintered onto the support of the used catalyst. Energy-dispersive X-ray (EDS) analysis on several parts of the investigated sample reveals the absence of Ru in some areas of the $SiO_2$ support, supporting the notion that Ru agglomerates under reaction conditions. This is in accordance with the BET results that suggested a reduction of the surface area after reaction due to agglomeration.

Finally, the silica and alumina-supported Ru catalysts prepared by chloride were also examined with TEM (Fig. 4), in order to compare with the corresponding nitrate-prepared catalysts and investigate the effect of the precursor on the structure of the materials. As aforementioned, the Ru/Si($NO_3$) catalyst exhibits a narrow particle size distribution (Fig. 2), with a mean particle size of 8.17 nm. The RuSi($Cl_3$) catalyst demonstrates slightly larger particles and exhibits a similar particle size distribution (Fig. 4) with an average particle size 8.23 nm and dispersion equal to 16.04%. In the case of the alumina-supported sample prepared with the chloride precursor the average particle size is 14.46 nm ($D$ = 9.12%), visibly larger than the corresponding for RuAl($NO_3$), as shown in Fig. 4. EDS of the sample Ru/Al($Cl_3$) revealed the presence of ~1% atomic residual $Cl^-$ ions residing only on the alumina support (Inset in Fig. 4). This result agrees with previous findings which showed that slightly smaller metal particles are attained on Cl-free catalysts [27]. It has been suggested that this could be attributed either to the speciation of the aqueous solution used, as $RuCl_3$ solutions contain polymeric species, and/or to sintering favoured in the presence of $Cl^-$ ions, which are retained on the support surface [28].

Metal dispersion was additionally determined by hydrogen chemisorption and subsequent temperature programmed desorption. The dispersion of the silica-supported catalysts could not be determined by this method, probably due to the low $H_2$ uptake at chemisorption temperatures in the range of 30–250 °C. The same was observed by Kellner and Bell [29]. Therefore, results for dispersion, as well as metal particle size, summarized in Table 1, are shown only for the catalysts supported on $\gamma$-$Al_2O_3$ and $ZrO_2$. It should be noted here that in general the Ru particle size measured with $H_2$-chemisorption is systematically found to be lower than the corresponding determined by TEM. According to literature, these differences arise from a spillover effect of hydrogen from the metal to the support, always present in chemisorption phenomena [30]. Indeed, the above mentioned was also observed in our case. For example on RuAl($NO_3$) catalyst the Ru particle size calculated from $H_2$-chemisorption (see Table 1) was found to be ~2 nm, much lower than the value of 13.55 nm that was determined by TEM measurements. Based on $H_2$-chemisorption the metal dispersion is as follows: RuZr($NO_3$) > RuAl($NO_3$) ≫ RuAl($Cl_3$). Higher dispersion of Ru metal on $ZrO_2$ support compared to $\gamma$-$Al_2O_3$ prepared with the same nitrate precursor has also been reported by Mitsui et al., who measured dispersion of Ru-supported catalysts by CO pulse chemisorption [31]. The low dispersion measured by TPD-$H_2$ in the case of RuAl($Cl_3$) compared with the RuAl($NO_3$) can be attributed to the residual chloride which has been reported to inhibit hydrogen chemisorption [32]. This could be an explanation for the discrepancy between the particle size difference measured with TEM and $H_2$ chemisorption for the alumina-supported Ru samples, as TEM-determined dispersion is very similar for the nitrate and chloride catalysts, while in the case of $H_2$-TPD the dispersion of RuAl($Cl_3$) is four times lower than that of RuAl($NO_3$).

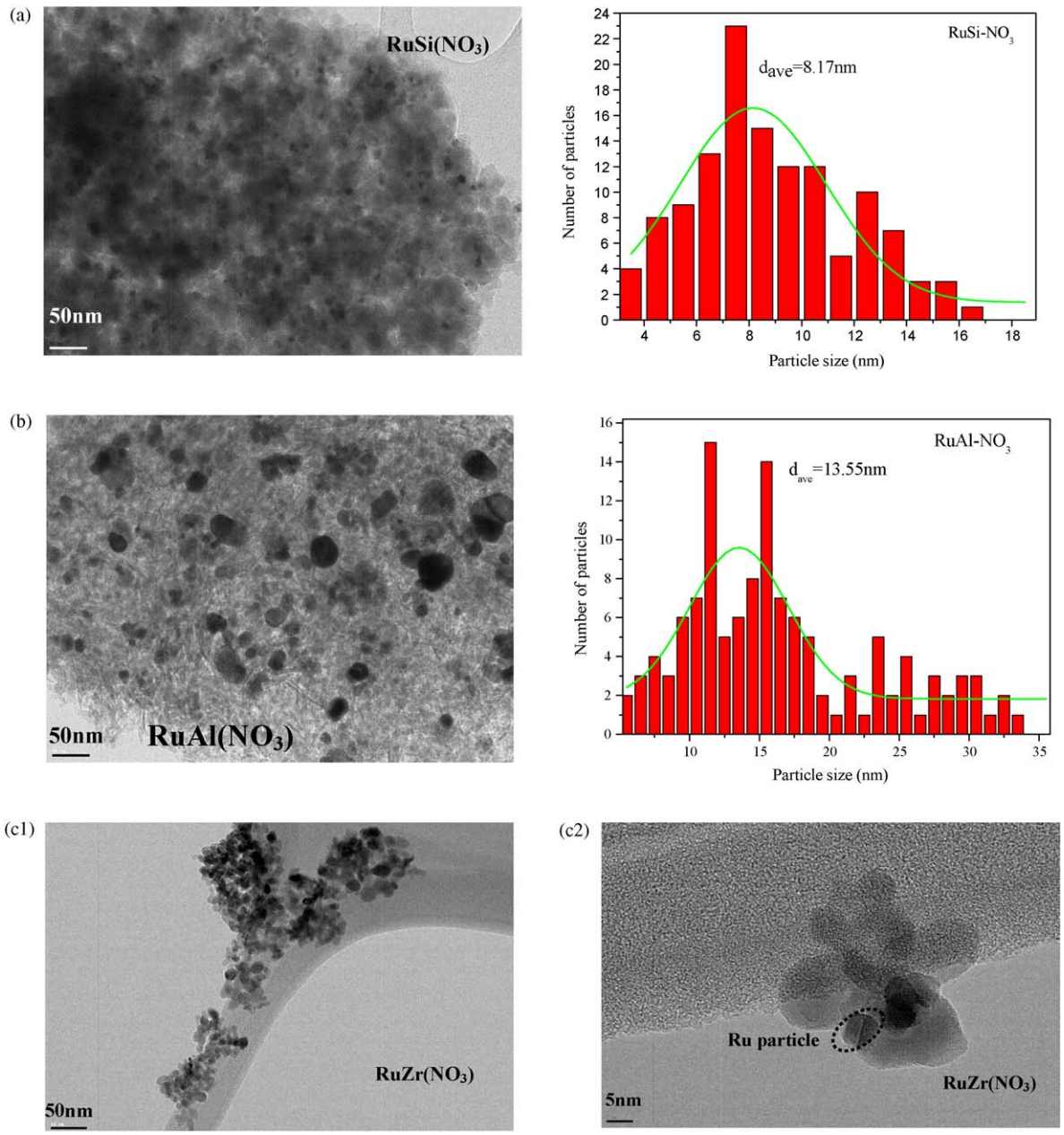


**Fig. 2.** TEM images of Ru-supported on (a) $SiO_2$, (b) $\gamma$-$Al_2O_3$ and (c1 and c2) $ZrO_2$ prepared with the nitrate precursor.

A previous reported dispersion value of 11% for 4 wt% $Ru/Al_2O_3$ prepared with the same $RuCl_3$ precursor is in agreement with our results [33].

Temperature programmed reduction was used to study the reducibility of the catalysts. Fig. 5 reports the hydrogen TPR profiles for the catalysts supported on $SiO_2$, $\gamma$-$Al_2O_3$ and $ZrO_2$ prepared with the two different Ru precursors. All catalysts, show one main reduction peak at 150–250 °C, while the $RuAl(Cl_3)$ sample exhibits additionally a broad shoulder at lower temperature. The main peak corresponds to the reduction of $RuO_2$ to metallic Ru. Unsupported bulk $RuO_2$ has been reported to reduce in a single peak at 217 °C [34]. Consequently, the main reduction peak is assigned to the reduction of $RuO_2$ to Ru, while the shoulder observed on $RuAl(Cl_3)$ has been related to the reduction of well-dispersed $RuO_x$ species [35,36]. Quantification of the $H_2$ uptake yields in all samples a value very close to the theoretical amount of hydrogen required for the total reduction of Ru ions from +4 to the metallic form. The reduction temperature increases in the order $ZrO_2 < SiO_2 < \gamma$-$Al_2O_3$, indicating that the support material greatly influences the reducibility of the Ru species. The stronger metal-support interaction reported for the $Ru/\gamma$-$Al_2O_3$ system may be the reason for the increased reduction temperature of the ruthenium species on alumina, compared with $SiO_2$ and $ZrO_2$ [30]. For the Ru catalysts prepared with different Ru metal precursors a difference at the reduction temperature is also observed. In both the $\gamma$-$Al_2O_3$ and $SiO_2$ supported samples, the chloride prepared catalysts are reduced at lower temperature. Additionally, Ru-supported on $\gamma$-$Al_2O_3$ prepared with the chloride precursor exhibits a broad shoulder at lower temperature, as mentioned above.

The acidic properties of the bare supports and the Ru catalysts were investigated with $NH_3$-TPD after saturation of the catalytic surface with ammonia at 100 °C. The ammonia desorption curves as well as the acidity values of the catalysts and the supports (expressed as μmol of desorbed $NH_3$/g) are compiled in Fig. 6. The

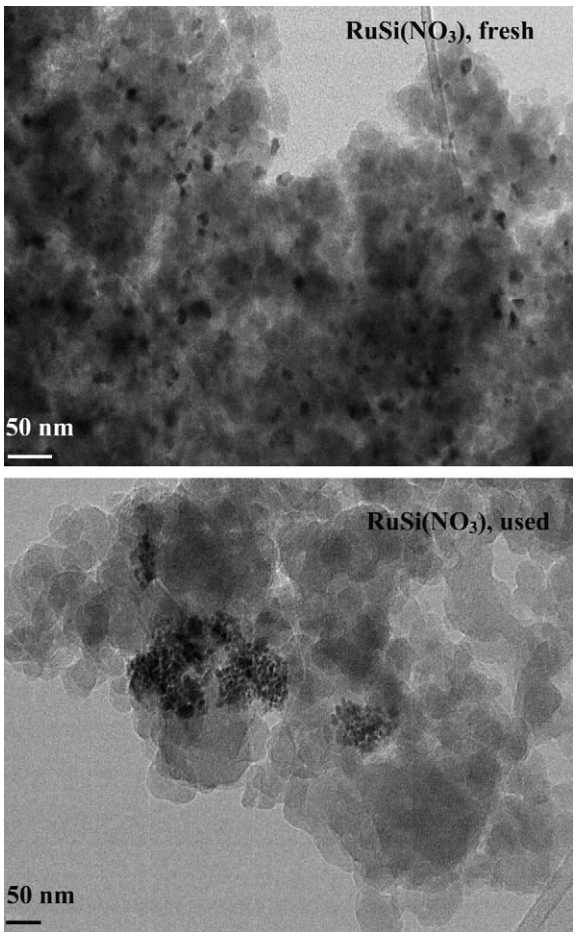


**Fig. 3.** TEM images of the $Ru/SiO_2$ catalyst fresh and used prepared with the nitrate precursor.

acidity values are also tabulated in Table 1. The concentration of acid sites decreases in the order $RuAl(Cl_3) > RuZr(NO_3) > RuAl(NO_3) > RuSi(Cl_3) > RuSi(NO_3)$ (see Table 1). In all Ru-based catalysts we observed a main ammonia desorption peak, lying in the 100–500 °C range for all catalysts, indicating the presence of weak/medium acid sites of similar strength. The $RuZr(NO_3)$ catalyst is characterized by a broad shoulder and a desorption peak, in the temperature range ~100–500 °C, with the maximum temperature peak at 300 °C. In contrast the $NH_3$-TPD of the $ZrO_2$ support showed a broad desorption peak, in the temperature range ~200–450 °C and a peak at higher temperature ~520 °C [37]. The $NH_3$-TPD profiles of Ru-supported on $\gamma$-$Al_2O_3$ are also characterized by a broad peak in the temperature range 170–500 °C, while the $\gamma$-$Al_2O_3$ support exhibits an additional peak at 660 °C related to acid sites of high strength [38]. The $Ru/SiO_2$ catalysts and the $SiO_2$ support demonstrate almost the same ammonia desorption pattern with a broad peak located in the temperature range 150–300 °C and a high temperature shoulder up to 500 °C [39]. As can be seen in Fig. 5, the high temperature peak present on $ZrO_2$ and $\gamma$-$Al_2O_3$ was not recorded on the $SiO_2$ support, indicating the absence of strong acid sites on silica as opposed to zirconia and alumina. Quantification of the amount of desorbed ammonia in all materials clearly demonstrates that the impregnation of Ru on all supports causes a significant decrease in total acidity. This is also visible in the ammonia patterns, as the high temperature peak of the $Al_2O_3$ and $ZrO_2$ disappears in the Ru samples. It can be thus postulated that Ru interacts strongly with the stronger acid sites of the support, which are covered by the metal species. Ru active species possibly reside on the strong acid sites of the support and as a consequence decrease the overall acidity of the as-prepared Ru-supported samples.

### 3.2. Catalytic results

The activity and selectivity of the supported Ru catalysts in the glycerol hydrogenolysis reaction was explored at 240 °C and 8 MPa initial hydrogen pressure. On all catalysts, the identified products were 1,2-propanediol, 1,3-propanediol, ethylene glycol, 1-propanol, 2-propanol, acetol, ethanol, methanol, $CH_4$, $CO_2$, CO, $C_2H_6$. The acetol indermediate was detected in all experiments, supporting the proposed [14,17–19] dehydration/hydrogenation mechanism for glycerol hydrogenolysis, according to which glycerol dehydrates to form the intermediate product acetol and subsequently hydrogenates to the desirable 1,2-propanediol.

The conversion of glycerol and selectivity to liquid products is tabulated in Table 2 for all samples under study. The results clearly show that the main reaction product of glycerol hydrogenolysis over Ru-supported catalysts, with the exception of the $RuAl(Cl_3)$ catalyst, is 1,2-propanediol, independent of the support or the metal precursor used. 1,3-Propanediol is produced in minor amounts only in the presence of the alumina-supported Ru samples. Ethylene glycol, derived from unselective primary degradation reactions of glycerol is also produced, while significant amounts of propanols produced from secondary hydrogenolysis of propanediols, are also formed. In all catalysts, except of $RuAl(Cl_3)$ the selectivity to propanols (1-, 2-propanol) is much lower than on Ru/C [19] and in the case of silica and zirconia Ru-supported catalysts (this study) the selectivity to propanols is lower than on Ru/C + Amberlyst also [19]. Gas products were detected in all cases and consisted mainly of methane, and minor amounts of ethane, $CO_2$ and CO.

The activity of the catalysts in glycerol conversion after 5 h reaction time is as follows: $RuAl(Cl_3) > RuZr(NO_3) > RuAl(NO_3) \sim RuSi(Cl_3) > RuSi(NO_3)$. Worthy to mention is the extremely high values of the intrinsic activity of the Ru sites expressed as TOF ($h^{-1}$) (Table 2). Even though these values cannot be directly compared with literature data, present data are about an order of magnitude higher than other reported frequency values of Ru catalysts [13]. The activity per Ru site seems to be highly dependent on the support used as the TOF values vary significantly up to a factor of 5. The acidic characteristics and/or the different metal particle sizes might influence the intrinsic rate of glycerol activation.

The order of 1,2-propanediol liquid-based selectivity at 20% glycerol conversion is: $RuSi(NO_3)$ (65%) > $RuZr(NO_3)$ (62.4%) > $RuSi(Cl_3)$ (54.6%) > $RuAl(NO_3)$ (52%) > $RuAl(Cl_3)$ (39.4%). Overall, Ru-supported on $Al_2O_3$ and prepared with a chloride precursor is the most active catalyst, while the silica supported sample prepared with a nitrate precursor proves to be the most selective material for the production of 1,2-propanediol.

#### 3.2.1. Effect of support

In this work the effect of the support material in glycerol hydrogenolysis reaction at 240 °C and 8 MPa hydrogen pressure was examined with Ru-supported on $\gamma$-$Al_2O_3$, $SiO_2$ and $ZrO_2$ and prepared with the same nitrate metal precursor. In terms of activity (see Table 2), Ru-supported on $Al_2O_3$ and $SiO_2$ yields similar glycerol conversion values of around 26.7% and 21.7% respectively. A more pronounced support effect is observed in the case of zirconia, where the activity increases significantly to a value of ~40.5%.

Besides activity, an essential characteristic of a good hydrogenolysis catalyst is the ability to promote the dehydration of glycerol to acetol and subsequent hydrogenation to the desired product, 1,2-propanediol, and suppress the degradation reactions

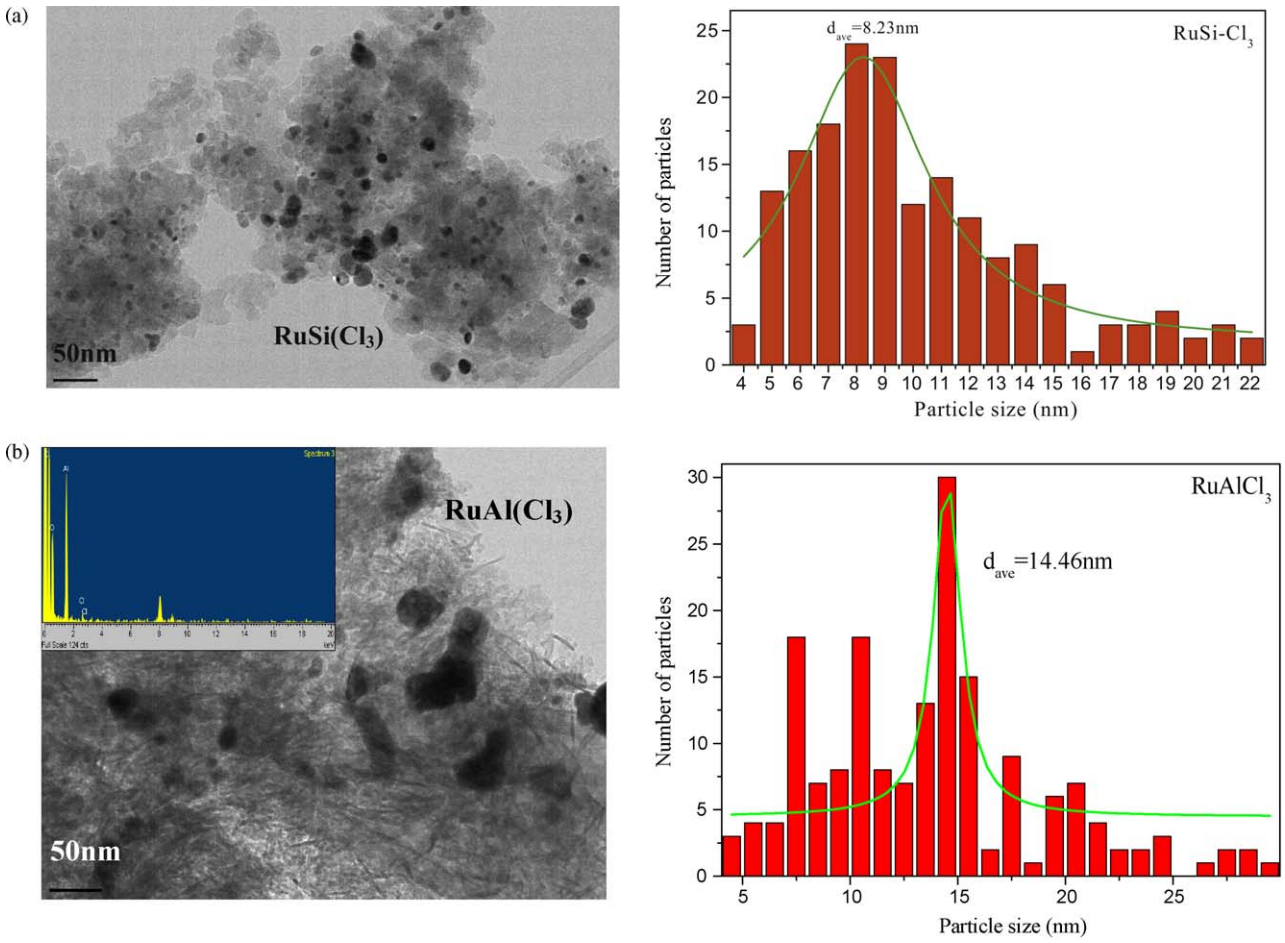


**Fig. 4.** TEM images of Ru-supported on (a) $SiO_2$ and (b) $\gamma$-$Al_2O_3$ prepared with a chloride precursor.

to ethylene glycol. Moreover, the catalyst should preserve the formed propanediol from consecutive hydrogenolysis to propanols. The effect of the different supports on product selectivity in glycerol hydrogenolysis is shown in Fig. 7. It should be noted that the presented liquid-based selectivity was calculated at 20% glycerol conversion. The results show that when Ru is supported on silica it exhibits the highest selectivity to 1,2-propanediol, with zirconia following closely and alumina demonstrating the worst selectivity results. The selectivity values of the main degradation product, ethylene glycols vary between ~23 and 30%. $RuAl(NO_3)$ and $RuSi(NO_3)$ similarly catalyze the C–C bond scission reactions as the selectivity values for ethylene glycol are very close, while $ZrO_2$ supported catalyst exhibits the lowest selectivity for ethylene glycol. A closer inspection of the product selectivity shows that the main difference in the product distribution that renders the silica catalyst more selective is the acetol intermediate product that readily hydrogenates to produce 1,2-propanediol on silica-supported catalyst. As shown in Fig. 7 the selectivity of acetol intermediate on silica supported catalyst is very low (~1%) compared to $\gamma$-$Al_2O_3$ and $ZrO_2$ supported samples. In addition, the silica-based Ru catalyst seems to prevent the excessive hydrogenolysis of 1,2-propanediol to propanols. The catalytic results (Fig. 7) reveal that the selectivity values for propanols on $RuAl(NO_3)$ and $RuZr(NO_3)$ are between 7 and 10%, while on silica supported Ru catalyst no propanols were detected. Feng et al. studied glycerol hydrogenolysis over pre-reduced Ru-supported catalysts on various supports ($TiO_2$, $SiO_2$, NaY, $\gamma$-$Al_2O$ and C). In agreement with our results, they found $Ru/SiO_2$ to be the most selective (55.2% selectivity to 1,2-PDO), but less active (3.1% conversion) catalyst [12].

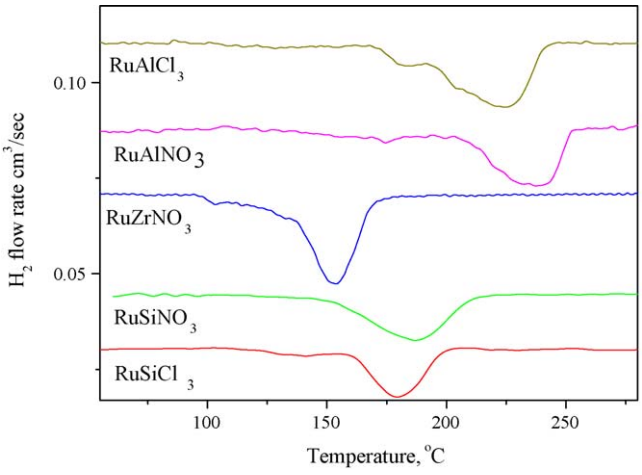


**Fig. 5.** Temperature programmed reduction profiles of Ru-supported catalysts.

Although in dehydration/hydrogenation reactions it is preferable not to use water in the initial feed in order to drive the equilibrium in the forward direction, very dilute aqueous glycerol solutions have been mainly used in previous literature reports [8,9,12–14,16–20]. Recent publications [40] investigating the effect of water in the feed report that significantly higher conversion levels are observed with pure glycerol compared to aqueous solutions, however selectivity to 1,2-propanediol

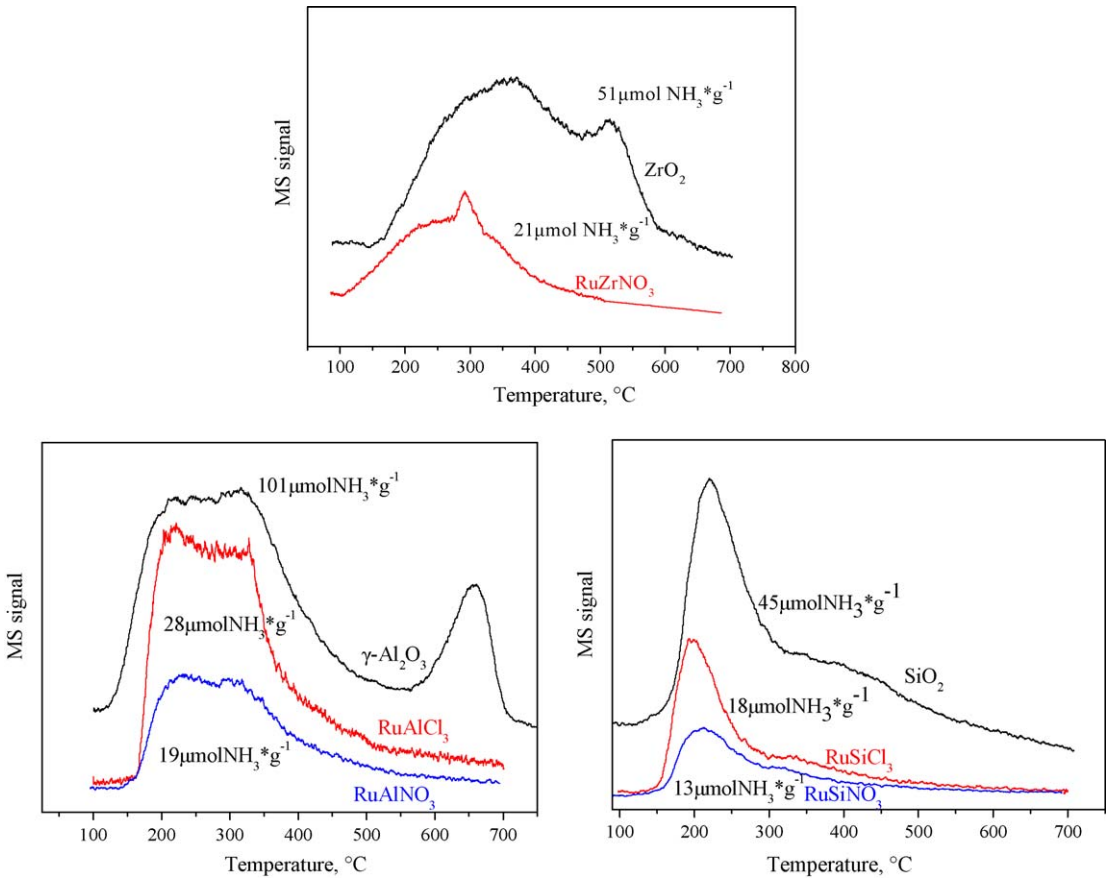


**Fig. 6.** TPD-$NH_3$ profiles of Ru-supported catalysts on γ-$Al_2O_3$, $SiO_2$ and $ZrO_2$.

**Table 2**
Catalytic results of glycerol hydrogenolysis over Ru-supported catalysts (reaction conditions: 8 MPa hydrogen pressure, 240 °C, 0.9 g catalyst, 120 ml pure glycerol, 5 h, stirring = 1000 rpm).

| Catalyst | Conversion, % | TOF ($h^{-1}$)[a] | Liquid-based selectivity, % (5 h) | | | | | | |
|---|---|---|---|---|---|---|---|---|---|
| | | | 1,2-PDO | 1,3-PDO | EG | acetol | Propanols (1-, 2-) | $C_1$–$C_2$ alcohols | $C_{4+}$ products |
| RuAl($Cl_3$) | 69.0 | 5591.7 | 37.9 | 0.7 | 10.4 | 2.5 | 45 | 0.3 | 3.2 |
| RuAl($NO_3$) | 26.7 | 2034.5 | 39.7 | 0.4 | 14 | 7.4 | 16 | 1.5 | 8.5 |
| RuSi($Cl_3$) | 25.2 | 1166.5 | 50.4 | – | 24.0 | 11 | 9 | 0.7 | 4.2 |
| RuSi($NO_3$) | 21.7 | 996.5 | 60.5 | – | 28.7 | 2.4 | 0 | 1.3 | 5.8 |
| RuZr($NO_3$) | 40.5 | 1248.9 | 60.5 | – | 21.9 | 6.4 | 7.1 | 0.6 | 3.6 |

[a] The TOF values were calculated from the conversion data of glycerol at 5 h based on the metal surface area, calculated from the dispersion values determined by TEM.

decreases. It is worth to mention that in our experiments pure glycerol and low catalyst/glycerol (0.0059) weight ratio were used at 5 h reaction time. The latter is very important considering that ruthenium is a high-cost noble metal. As an example, Alhanash et al. [9] report a glycerol conversion of only 21% at 150 °C after 10 h reaction time over a 5% Ru/$Cs_{2.5}H_{0.5}[PW_{12}O_{40}]$ catalyst although they use very dilute glycerol solutions as feedstock and ~32 times higher catalyst/glycerol weight ratio(0.192) than the ratio used in the present report. Considering all the above, it is clear that the Ru catalysts synthesized and tested in this work exhibit very high activity at low catalyst/feed ratios and very high selectivity to 1,2-propanediol (~65%) even with the use of pure glycerol as feed.

### 3.2.2. Effect of metal precursor

The effect of the metal precursor on the performance of Ru-supported catalysts on γ-$Al_2O_3$ and $SiO_2$ was studied. As mentioned earlier, Ru metal was loaded on the support using two metal precursors: $RuNO(NO_3)_3$ and $RuCl_3 \cdot xH_2O$. Fig. 8 presents product selectivities at isoconversion for the four catalysts evaluated in the glycerol hydrogenolysis reaction at 240 °C and 8 MPa $H_2$ pressure. As shown from the results, the different metal precursor mainly affects the performance of the catalyst when supported on γ-$Al_2O_3$. Comparing the two materials, RuAl($Cl_3$) and RuAl($NO_3$), we can see that the catalyst is almost twice as active when prepared with the chloride precursor, but selectivity to the desired product 1,2-propanediol drops significantly. This drop in selectivity on RuAl($Cl_3$) is accompanied by the formation of propanols. Propanols are products of the secondary hydrogenolysis of 1,2-propanediol and/or 1,3-propanediol which is apparently catalyzed by the Ru catalyst prepared with chloride leading to decreased propanediol selectivity. This behaviour can be attributed to the presence of residual $Cl^-$ ions on the RuAl($Cl_3$) catalyst. It is well known from literature that γ-$Al_2O_3$ easily incorporates chloride into its structure [41]. This was confirmed by TEM-EDS where almost 1% atomic residual chloride was detected in the case of the RuAl($Cl_3$) catalyst. The incorporation of chloride in the RuAl($Cl_3$) catalyst causes a significant increase in the acidity of

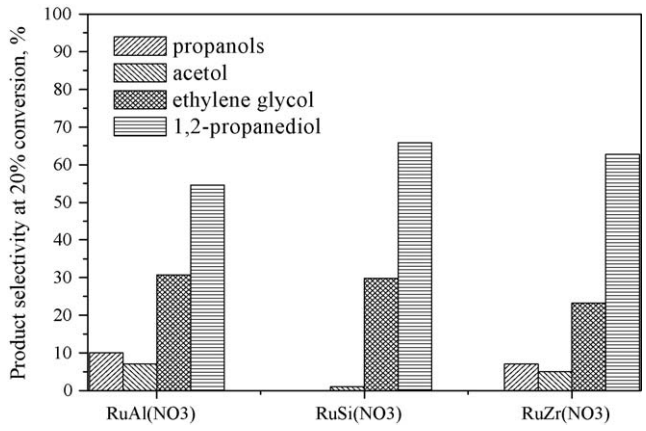


**Fig. 7.** Effect of support on product selectivity at 20% glycerol conversion (experimental conditions: $T = 240\ ^{\circ}C$, $P_{H_2} = 8$ MPa, 0.9 g catalyst, 120 ml pure glycerol, 5 h, stirring = 1000 rpm).

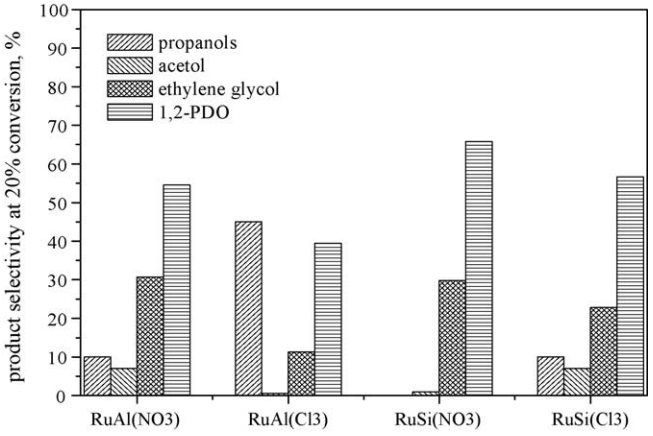


**Fig. 8.** Effect of metal precursor on product selectivity at 20% glycerol conversion (experimental conditions: $T = 240\ ^{\circ}C$, $P_{H_2} = 8$ MPa, 0.9 g catalyst, 120 ml pure glycerol, 5 h, stirring = 1000 rpm).

the catalyst compared to the RuAl($NO_3$) sample, as shown by the acidity measurements in Table 1. The increased acidity, due to the presence of $Cl^-$ ions, seems to be responsible for the high activity of RuAl($Cl_3$) and the promotion of the secondary hydrogenolysis reaction of 1,2-propanediol to propanols [28].

Unlike alumina, silica does not incorporate chloride into its structure as strong as alumina does and as a result the effect of the metal precursor on silica supported catalysts is less noticeable [42]. The catalytic results show that the activity of RuSi($Cl_3$) is higher than (RuSi$NO_3$) catalyst (Table 2), but the chloride prepared sample promotes 1,2-PDO hydrogenolysis to propanols. On the contrary RuSi($NO_3$) catalyst prevents the excessive hydrogenolysis of the desirable product (0% selectivity to propanols) resulting in higher selectivity to 1,2-PDO. This is related to the lower acidity of the nitrate-prepared Ru/$SiO_2$ catalyst that limits the sequential dehydration of 1,2-propanediol, which proceeds on the acidic sites of the catalytic material.

### *3.2.3. Correlation of catalyst physicochemical properties and catalytic behaviour*

It has been well established that hydrogenolysis reaction over supported noble metal catalysts is strongly influenced by the acidity of the support material [42,43]. Tomishige and co-workers examined hydrogenolysis reaction in the presence of solid acids and especially Amberlyst ion-exchange resins. They found that the addition of a solid acid enhances glycerol conversion in combination with Ru/C or Rh/$SiO_2$ [14,17–19]. The influence of solid acids on glycerol hydrogenolysis was also studied by Balaraju et al. [43] in the presence of Ru/C and various solid acids as co-catalysts. Their results showed that the conversion of glycerol depends on the total acidity and that a linear correlation between these two properties exists.

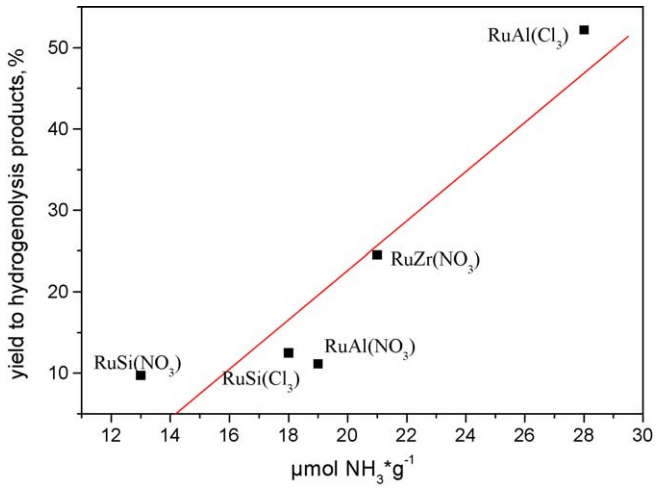


**Fig. 9.** Glycerol conversion to hydrogenolysis products as function of the acidity of the catalytic materials.

In agreement with their observations, our results indicate the same correlation of glycerol conversion to hydrogenolysis products (1,2-propanediol, 1,3-propanediol, 1-propanol, 2-propanol) with the catalyst acidity. The as-prepared Ru-supported catalysts were characterized by $NH_3$-TPD in order to determine their acidity and the results are shown in Table 1. A clear correlation between glycerol yield to hydrogenolysis products and acidity is apparent, as shown in Fig. 9. Glycerol conversion to hydrogenolysis products increases with the total acidity of the catalytic materials. Moreover, as only acid sites of weak/medium strength were observed on the Ru catalysts supported on $Al_2O_3$, $SiO_2$ and $ZrO_2$, the results suggest that moderate acid sites are sufficient to activate glycerol dehydration, in agreement with previous literature reports [43] and therefore the total amount of acid sites is important and influences the rate of the reaction. However it should be stressed that the presence of the metal is essential for the activation of glycerol. Tests with the bare supports under the typical conditions used in this study resulted in very low conversion (<3%), even though the supports themselves exhibit a much higher acidity than the Ru samples. This implies that while dehydration does proceeds on the acidic sites, the presence of the metal is crucial for the extent even of the first step. Present results suggest that this dual metallic/acidic function consists the key parameter for the efficient hydrogenolysis of glycerol to 1,2-propanediol.

## 4. Conclusions

The results of this study indicate that Ru-based on oxide supports are very effective catalysts for pure glycerol hydrogenolysis. The Ru-supported on silica with the use of the nitrate precursor showed the highest selectivity to 1,2-propanediol of 65% at 20% glycerol conversion. The TOF values of these materials are very high and the differences between them indicate that the support material strongly influences the activity per Ru site. The use of different metal precursor has an effect on both alumina and silica supported catalysts due to the incorporation of $Cl^-$ ions in the support and the increase of the acidity compared to the nitrate-prepared samples. This increased acidity is responsible for the additional promotion of the excessive hydrogenolysis of the

desired 1,2-propanediol to propanols. Yield to hydrogenolysis products strongly correlates with the total acidity of the catalysts, as our results clearly show a linear relation. This work can conclude that the presence of the metallic surface and the acidic function of the Ru-based catalysts is of great importance for the hydrogenolysis reaction to perform.

## Acknowledgements

The authors gratefully acknowledge Dr Andreas Delimitis and Mrs Thaleia Vavaleskou from CPERI/CERTH for their help in XRD, SEM and TEM measurements.

## References

[1] F. Ma, M.A. Hanna, Biores. Technol. 70 (1) (1999) 1.
[2] W. Weirauch, Hydro. Proc. 87 (2008) 23.
[3] R.S. Karinen, A.O.I. Krause, Appl. Catal. A: Gen. 306 (2006) 128.
[4] Werpy, G. Petersen, vol.1 Results of Screening for Potential Candidates from Sugars and Synthesis Gas, US DOE Report, 2004.
[5] R.D. Cortright, M. Sanchez-Castillo, J.A. Dumesic, Appl. Catal. B: Environ. 39 (2002) 353.
[6] J. Chaminand, L.A. Djakovitch, P. Gallezot, P. Marion, C. Pinel, C. Rosier, Green Chem. 6 (8) (2004) 359.
[7] M.A. Dasari, P.P. Kiatsimkul, W.R. Sutterlin, G.J. Suppes, Appl. Catal. A: Gen. 281 (1–2) (2005) 225.
[8] S. Wang, H. Liu, Catal. Lett. 117 (1) (2007) 62.
[9] A. Alhanash, E. Kozhevnikova, V. Kozhevnikov, Catal. Lett. 120 (2008) 307.
[10] T. Kurosaka, H. Maruyama, I. Naribayashi, Y. Sasaki, Catal. Commun. 9 (6) (2008) 1360.
[11] L. Huang, Y.-L. Zhu, H.-Y. Zheng, Y.-W. Li, Z.-Y. Zeng, Chem. Technol. Biotechnol. 83 (2008) 1670.
[12] J. Feng, H. Fu, J. Wang, R. Li, H. Chen, X. Li, Catal. Commun. 9 (6) (2008) 1458.
[13] E.P. Maris, R.J. Davis, J. Catal. 249 (2007) 328.
[14] T. Miyazawa, S. Koso, K. Kunimori, K. Tomishige, Appl. Catal. A: Gen. 318 (2007) 244.
[15] D.G. Lahr, B.H. Shanks, J. Catal. 232 (2) (2005) 386.
[16] E.P. Maris, W.C. Ketchie, M. Mitsuhiro, D.J. Robert, J. Catal. 251 (2) (2007) 281.
[17] I. Furikado, T. Miyazawa, S. Koso, A. Shimao, K. Kunimori, K. Tomishige, Green Chem. 9 (6) (2007) 582.
[18] T. Miyazawa, S. Koso, K. Kunimori, K. Tomishige, Appl. Catal. A: Gen. 329 (2007) 30.
[19] T. Miyazawa, Y. Kusunoki, K. Kunimori, K. Tomishige, J. Catal. 240 (2) (2006) 213.
[20] J. Feng, J. Wang, Y. Zhou, H. Fu, H. Chen, X. Li, Chem. Lett. 36 (10) (2007) 1274.
[21] T.M. Che Tessie, US Patent 4,642,394 (1987).
[22] E. Drent, W.W. Jager, US Patent 6,080,898 (2000).
[23] G.J. Suppes, W.R. Sutterlin, EPO, WO 2007053705 (2007).
[24] C. Montassier, J.C. Menezo, L.C. Hoang, C. Renaud, J. Barbier, J. Mol. Catal. 70 (1991) 99.
[25] J.R. Anderson, Structure of Metallic Catalysts, Academic Press Inc., New York, 1975 , p. 295.
[26] J.W. Da-Silva, A.J.G. Cobo, Appl. Catal. A 252 (2003) 9.
[27] N. Li, C. Descorme, M. Besson, Appl. Catal. B: Environ. 71 (2007) 262.
[28] B. Bachiller-Baeza, A. Guerrero-Ruíz, I. Rodríguez-Ramos, J. Catal. 229 (2005) 439.
[29] C.S. Kellner, A.T. Bell, J. Catal. 71 (1981) 288.
[30] M.G. Cattania, F. Parmigiani, V. Ragaini, Surf. Sci. 211/212 (1989) 1097.
[31] T. Mitsui, K. Tsutsui, T. Matsui, R. Kikuchi, K. Eguchi, Appl. Catal. B: Environ. 81 (2008) 56.
[32] T. Narita, H. Miura, M. Ohira, H. Hondou, K. Sugiyama, T. Matsuda, R.D. Gonzalez, Appl. Catal. 32 (1987) 185.
[33] V. Mazzieri, N. Fígoli, F.-C. Pascual, P. L' Argentiere, Catal. Lett. 102 (1–2) (2005) 79.
[34] P.G.J. Koopman, A.P.G. Kieboom, H. van Bekkum, React. Kinet. Catal. Lett. 8 (1978) 389.
[35] R. Lanza, S.G. Jaras, P. Canu, Appl. Catal. A: Gen. 325 (2007) 57.
[36] C.T. Williams, C.G. Takoudis, M.J. Weaver, J. Phys. Chem. B 102 (1998) 406.
[37] T. Finke, M. Gernsbeck, U. Eisele, C. Vincent, M. Hartmann, S. Kureti, H. Bockhorn, Therm. Act. 473 (2008) 32.
[38] E. Heracleous, A.A. Lemonidou, J.A. Lercher, Appl. Catal. 264 (2004) 73.
[39] J. Gao, J. Guo, D. Liang, Z. Houa, J. Fei, X. Zheng, Int. J. Hydrogen Energy 33 (2008) 5493.
[40] L.C. Meher, R. Gopinath, S.N. Naik, A.K. Dalai, Ind. Eng. Chem. Res 48 (2009) 1840.
[41] T. Narita, H. Miura, K. Sugiyama, T. Matsuda, D. Richard, Gonzalez, J. Catal. 103 (1987) 492.
[42] Y. Zhang, M. Toebes, K.P. de Jong, D.C. Koningsberger, in: Proceedings of the 19th North American Meeting Philadelphia, May, 2005.
[43] M. Balaraju, V. Rekha, P.S.S. Prasad, B.L.A.P. Devi, R.B.N. Prasad, N. Lingaiah, Appl. Catal. A: Gen. 354 (2008) 82.